Biomass Conversion and Biorefinery
https://doi.org/10.1007/s13399-022-03319-x

ORIGINAL ARTICLE

Modeling and optimization of the adsorptive removal of crystal violet dye by durian (*Durio zibethinus*) seeds powder: insight into kinetic, isotherm, thermodynamic, and adsorption mechanism

Nur Aimi Jani[1] · Larbi Haddad[2] · Ahmed Saud Abdulhameed[3,4] · Ali H. Jawad[1] · Zeid A. ALOthman[5] · Zaher Mundher Yaseen[6,7]

Received: 13 June 2022 / Revised: 1 September 2022 / Accepted: 19 September 2022

Abstract

In this study, a renewable and effective bio-adsorbent was derived from Malaysian durian seeds (DSs) to act as a promising biosorbent for phytoremediation application towards removal of a hazardous cationic dye (crystal violet, CV) from aqueous environments. The physiochemical characteristics of DS were investigated by several analytical methods such as FTIR, TGA-DTG, BET, pH_{pzc}, and SEM-EDX. Subsequently, a statistical optimization for CV removal by DS was carried out via Box-Behnken design (BBD) and numerical desirability function. In this regard, four operational factors that affect CV adsorption, i.e., DS dosage (0.02–0.1 g), initial pH (4–10), temperature (25–50 °C), and adsorption time (5–25 min) were optimized by BBD and numerical desirability function. Hence, the highest CV removal (93.91%) was recorded under the optimal conditions found through desirability function as follows: DS dosage of 0.081 g, solution pH = 9.9, working temperature = 34.6 °C, and contact time = 24.9 min. Furthermore, ANOVA test indicated the significant parametric interactions towards CV removal (%) can be observed between AB (DS dose *vs*. initial pH), AD (DS dose *vs*. time), and BC (initial pH *vs*. temperature) interactions. The adsorption kinetic process was well described by a pseudo-second-order model. Subsequently, the adsorption equilibrium isotherm was well presented by Freundlich and Temkin isotherm models with maximum adsorption capacity of 158 mg/g. Thus, the thermodynamic functions revealed that the adsorption process was spontaneous and endothermic in nature. The adsorption mechanism of CV on the DS surface can be ascribed to the electrostatic forces, *n*-π stacking, and H-bonding interactions. Thus, the output of the research work indicates the potential applicability of DS as a renewable and effective biosorbent for the removal of CV from aqueous environments.

Keywords Durian seed · Biomass · Adsorption · Crystal violet dye · Box-Behnken design

1 Introduction

The discharge of industrial effluents generated from numerous sectors including paints, plastics, papers, leathers, and textiles in water bodies is becoming one of the most critical environmental concerns because of their negative effects on both humans and aquatic species [1]. Additionally, the physicochemical properties of freshwater such as color, odor, and pH are also altered after its contamination by organic dyes [2]. Moreover, the complex

✉ Ali H. Jawad
ali288@uitm.edu.my; ahjm72@gmail.com

1 Faculty of Applied Sciences, Universiti Teknologi MARA, 40450 Shah Alam, Selangor, Malaysia

2 Department of Chemistry, Faculty of Exact Sciences, University of Echahid Hamma Lakhdar – El/Oued, 39000 El Oued, Algeria

3 Department of Medical Instrumentation Engineering, Al-Mansour University College, Baghdad, Iraq

4 College of Engineering, University of Warith Al-Anbiyaa, Karbala, Iraq

5 Chemistry Department, College of Science, King Saud University, Riyadh 11451, Saudi Arabia

6 UniSQ's Advanced Data Analytics Research Group, School of Mathematics Physics and Computing, University of Southern Queensland, Springfield Central, QLD 4300, Australia

7 New era and Development in Civil Engineering Research Group, Scientific Research Center, Al-Ayen University, Thi-Qar 64001, Baghdad, Iraq

Published online: 27 September 2022

aromatic structures of the synthetic dyes mark them as poisonous, phototoxic, ototoxic, and possibly carcinogenic substances [3]. Therefore, the presence of the toxic organic and synthetic dyes in the aquatic system can cause harmful influence on the living things and entire eco-system [4–6].

Among various cationic dyes, Crystal Violet (CV; Basic violet 3, gentian violet, and methyl violet 10B are other names for CV) is a chemically synthesized cationic dye that belongs to the triphenylmethane family. It is widely utilized in various industrial applications such as dyeing, paper, textile, ink, additives, leather, cosmetics, and analytical chemistry/biochemistry, dermatological agents, biological staining, dye manufacture, and veterinary medicine [7–9]. The danger of this dye lies in its easy penetration into animal cells by interacting with negatively charged molecules from the membrane cells of mammals [10]. Furthermore, CV can also cause several harmful effects on human health such as skin irritation, digestive tract, conjunctiva, permanent injury to the cornea, and eye irritation [11, 12].

Thus, due to the harmful effects of CV on ecosystems, wastewater containing CV has become a target for remediation studies. For this reason, a variety of biological and physicochemical approaches including reverse osmosis [13], precipitation [14], coagulation/flocculation [15], ion exchange [16], membrane filtration [17], adsorption [18], and photo-Fenton oxidation [19] have been effectively implemented in wastewater treatment. However, each of these methods has several drawbacks, including extremely severe reaction conditions, high cost, low efficiency, incomplete removal, formation of hazardous intermediates, and time-consuming processes [20]. In this regard, adsorption process presents itself as a potential alternative over other conventional technologies due to its high efficiency even at high dye concentrations, selectivity, recyclability, cost-effectiveness, ease of operation, and broad applicability [21, 22].

From the adsorbent standpoint, several adsorbents have been reported for the adsorptive removal of dyes, for instance, guar gum/activated carbon nanocomposite [23], layered double hydroxides [24], hen feather [25], metal/halide-free ordered mesoporous carbon [26], ordered mesoporous carbon [27], sulfonated pomegranate peel biochar [28], chitosan/carbon-doped TiO_2 composite [29], Ag-doped MnO_2 (AgMC) nanocomposites [30], immobilized chitosan [31], and TiO_2 Degussa P25 [32]. One of the most utilized adsorbents for dye removal is activated carbon [33]. However, the main limitations of activated carbon application in the wastewater treatment methods come from its high operating costs of activation, functionality, and obtaining high porosity [34]. In light of these considerations, alternative materials such as natural and vegetal adsorbents have been applied as renewable, cost-effective, and efficient adsorbents [35–37]. Since it is known as the most inexpensive, renewable, and feasible choice for dye removal, biomass wastes have been fully exploited as adsorbents [38].

Furthermore, utilizing bio-wastes for the removal of various water pollutants is considered an eco-friendly, economical, and cost-effective approach for environmental remediation due to the several advantages such as the low cost, renewability, functionality, high efficiency, and compliance with green chemistry principles [39, 40]. In the previous few years, vegetal seeds such as spiky sweetgum tree seeds [41], Delonix regia seeds [42], Moringa seeds [43], mango seed [44], and *Dialium guineense* seed [45] have been successfully utilized as biosorbents for dye removal from aqueous environments. In this respect, Durian (*Durio zibethinus*), generally known as the "king of fruits," is a dicotyledonous tropical seasonal plant species [46]. Malaysia ranked second behind Thailand as a major producer of durian [47]. The average weight of durian fruit production across Malaysia is 255,353 metric tons, and the landfill loading rate is growing, due to the huge number and volume of durian waste, which needs more space to manage [48].

To the best of our knowledge, durian seed has never been applied in wastewater remediation. Therefore, the main objective of this research work is to utilize durian seeds (DSs) as biomass wastes to act as a promising biosorbent for the removal of toxic organic dyes such as crystal violet (CV) from aqueous environments. Thus, the adsorptive performance of DS towards capturing CV dye was statistically optimized by using response surface methodology-Box-Behnken design (RSM-BBD). Furthermore, the numerical desirability function was adopted to validate the statistical output of the response and to confirm the optimum operational condition of the adsorption, i.e., DS dose, solution pH, contact time, and working temperature. The physicochemical and adsorptive properties of DS were examined before and after CV adsorption. Subsequently, the adsorption kinetics, isotherms, and thermodynamic functions were determined. Besides that, a plausible mechanism for CV dye adsorption on the surface of DS was proposed.

2 Materials and methods

2.1 Materials

Durian was acquired at a local market in Shah Alam, Malaysia. Durian seeds (DSs) were first extracted, cleaned, and thoroughly rinsed in ultra-pure water. After that, the seeds were dried at 105 °C for 24 h to remove all traces of moisture. Finally, the dried seeds were crushed and sieved to a particle size of 1–2 mm. CV stock solution (1000 mg/L, R&M

Chemicals; λ_{max} = 584 nm; M.W = 408g/mol; R&M Chemicals) was prepared and diluted as needed for removal tests. R&M Chemicals supplied chemical reagents such as sodium chloride powder, sodium hydroxide pellets, and hydrochloric acid. The CV solutions, as well as the adsorption studies, were conducted using deionized water. Pure and analytical-grade chemicals were employed in this work.

2.2 Characterization

The surface parameters (pore volume and specific surface area) of DS were determined employing the analyzer Micromeritics ASAP 2060 using N_2 adsorption-absorption isotherms at temperature 77 K. The thermal stability of DS during the carbonization and activation process was determined by thermal analysis (NETZSCH STA 449 F5 Jupiter®). Under an atmosphere of N_2, measurements (thermograms) were generated between 30 °C/(10.0 K/min)/1200 °C. Chemical functional groups present in DS were examined before and after CV adsorption using PerkinElmer Spectrum RX I (RX-1, USA) Fourier transform infrared spectroscopy (FT-IR). The substances were prepared for FTIR analysis using KBr pellets. The Zeiss Supra 40VP scanning electron microscope (SEM) was used to examine the superficial morphology of DS before and after loading CV molecules on its surface, while the fundamental elements were detected using energy-dispersive X-ray (EDX). After mounting the samples on stubs, a gold-coating device was utilized to coat them with gold. High-resolution SEM pictures were then obtained by performing a SEM analysis at 15.0 keV. The pH at the point of zero charge (pH_{pzc}) for DS was acquired as per the previous work [49].

2.3 Design of experiments

The optimized removal of CV using DS as a biosorbent was investigated in this study using a four-level BBD model by changing the adsorbent dose, contact time, solution pH, and temperature as the independent variables in the BBD model. Subsequently, each variable was adjusted at three conventional levels: + 1, 0, and − 1 corresponding to high, medium, and low values, respectively. To be able to build the desired statistical model, the removal efficiency (R, %) was chosen as the response (Y). Thus, the statistical analysis was performed using the software Design-expert version 13.0 Stat-Ease to determine the relevance of each individual element, important interactions, and quadratic terms. The coded and actual values of the independent factors are depicted in Table S1. A non-linear regression model was used to fit the 2nd polynomial function to the empirical data and identify the essential model terms. The quadratic response model including all linear terms, linear by linear interaction items, and square terms is presented in Eq. (1):

$$Y = \beta_0 + \sum \beta_i X_i + \sum \beta_{ii} X_i^2 + \sum \sum \beta_{ij} X_i X_j \quad (1)$$

where Y, β_0, β_i, β_{ii}, β_{ij}, and (X_i and X_j) denote the response to be optimized, the constant coefficient, the linear coefficient, the quadratic coefficient, the interaction coefficient, and independent factors, respectively. As a result, twenty-nine BBD experiments were carried out to show and evaluate the influence of various input factors, i.e., A: DS (0.02–0.1 g), B: pH (4–10), C: temperature (25–50 °C), and D: time (5–25min) on the removal (%) of CV dye. Hence, Table 1 shows the limits of the studied variables as well as the corresponding calculated response (CV removal (%)). Thenceforth, the adsorption experiments of CV dye were carried out in batch mode in 250-mL capped Erlenmeyer flasks containing 100 mL of CV dye solutions. The batch adsorption experiments were carried out at a stirring speed of 100 strokes/min by means of a water bath shaker (Memmert, model WNB7-45, Germany). Subsequently, to achieve DS-free solutions, the samples taken from the dye solutions were filtered *via* a syringe filter (0.45 µm). The absorbance readings at different concentrations of CV solutions were monitored by Direct Reading spectrophotometer (HACH DR 3900, USA) at λ_{max} 584 nm. Then, the removal efficiency (R %) of the CV dye was calculated (Eq. S1).

2.4 Adsorption study of CV dye on DS

Batch adsorption study was conducted to measure the amount of dye adsorbed onto the DS surface, and the optimum operational conditions were determined based on the numerical desirability function. Consequently, the best operational conditions for maximum CV removal (93.9 %) were found to be DS dosage = 0.081 mg/L, pH = 9.9, temperature = 34.6 °C, and time = 24.9 min. Therefore, the adsorption study was carried out under these optimal conditions, with various CV initial concentrations (50–300 mg/L) and contact time (0–180 min). The batch adsorption experiments for CV dye were performed using the same method as outlined in "Design of experiments." Consequently, the amount of dye adsorbed onto the DS at equilibrium (q_e, mg/g) was determined (Eq. S2).

3 Results and discussion

3.1 3Characterization of DS

The surface properties of DS including specific surface area, mean pore diameter, and total pore volume are summarized in Table S2. The specific surface area of DS is 0.1096 m^2/g.

Table 1 The four-variable BBD matrix and experimental data for CV removal (%)

Run	A: DS dose (g)	B: pH	C: Temperature (°C)	D: Time (min)	CV removal (%)
1	0.02	4	37.5	15	14.3
2	0.1	4	37.5	15	61.9
3	0.02	10	37.5	15	27.6
4	0.1	10	37.5	15	93.8
5	0.06	7	25	5	40.9
6	0.06	7	50	5	58.8
7	0.06	7	25	25	58.3
8	0.06	7	50	25	67.5
9	0.02	7	37.5	5	24.5
10	0.1	7	37.5	5	62.7
11	0.02	7	37.5	25	25.9
12	0.1	7	37.5	25	88.8
13	0.06	4	25	15	40.6
14	0.06	10	25	15	64.9
15	0.06	4	50	15	40.7
16	0.06	10	50	15	87.9
17	0.02	7	25	15	20.7
18	0.1	7	25	15	82.3
19	0.02	7	50	15	38.6
20	0.1	7	50	15	90.9
21	0.06	4	37.5	5	25.3
22	0.06	10	37.5	5	58.3
23	0.06	4	37.5	25	38.5
24	0.06	10	37.5	25	81.1
25	0.06	7	37.5	15	55.1
26	0.06	7	37.5	15	58.4
27	0.06	7	37.5	15	52.3
28	0.06	7	37.5	15	60.5
29	0.06	7	37.5	15	54.6

Furthermore, its average pore diameter is 71.29 nm. According to the International Union of Pure and Applied Chemistry (IUPAC), the structure of DS is macroporous (average pore diameter ˃ 50 nm) [50].

The thermal degradation profile of the DS biomaterial was determined using a TGA-DTG test. The TGA-DTG curves of DS are presented in Fig. S1. The pyrolysis process of the DS biomass can be divided into two main stages. At 180 °C, the first weight loss of 11.09 % of DS occurred owing to loss of moisture and decomposition of high volatile components. The large fraction and most significant weight loss of 84.56 % of DS occurred in the range of 200–600 °C owing to the more stable volatile substances and hemicellulose decomposition [51]. Furthermore, cellulose breakdown, which is a fundamental structural component of DS, occurs at this stage. Finally, at this stage, the degradation of highly thermally stable lignin, as well as the creation of biochar, is achieved. The thermal degradation curve for the DS material is consistent with the thermal decomposition profile of DS reported earlier in terms of fractions of weight loss in the material [51]. In fact, the availability of functional groups on an adsorbent material provides more adsorption sites and therefore increases the adsorbed quantity of a pollutant [52]. For this reason, the FTIR spectral analysis on DS before and after adsorption of CV was carried out, and the spectra are given in Fig. 1a and b, respectively. The FTIR peaks shown in Fig. 1a reflected a number of functional groups based on their specific wavenumber positions (cm^{-1}). Figure 1a illustrates three peaks at 3650 cm^{-1}, 3617 cm^{-1}, and 3570 cm^{-1}, which are characteristic peaks to the stretching vibration of O–H in hydroxyl groups related to the alcohol, phenol, and carboxylic acids [53]. The weak peak at about 2927 cm^{-1} is allocated to the stretching vibration of the asymmetric C–H in methylene and methyl groups [54]. The stretching vibration of C≡C (alkynes) appeared at a peak at around 2280 cm^{-1} [55]. The peak at 1730 cm^{-1} is due to the C=O stretching of aldehyde, ester, ketone, and carboxylic acid [51]. Peaks at 1570 cm^{-1} and 1361 cm^{-1} are ascribed to

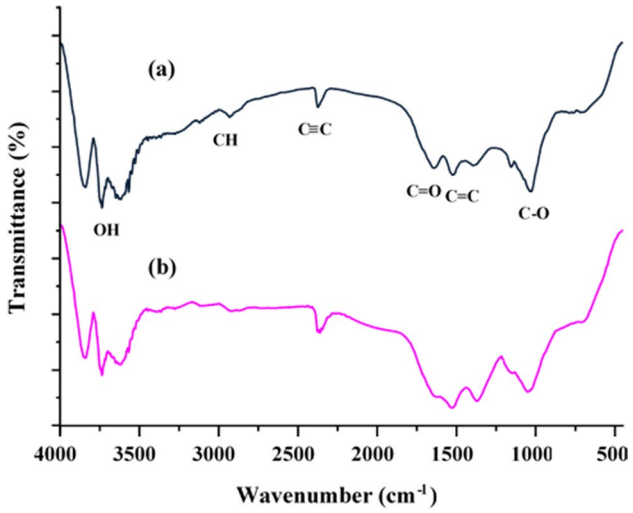

Fig. 1 FTIR spectra of (**a**) DS and (**b**) DS after adsorption of CV dye

C=C stretching and C–H stretching in alkanes or an alkyl group, respectively [55]. The peak at 1014 cm^{-1} covers the C–O–C groups stretching in ether, ester, or phenyl groups. Additionally, the symmetric stretching vibration of the carboxylate is also responsible for the formation of a 1470-cm^{-1} band; C–N is detected at band 1240 cm^{-1}, and the band at 1041 cm^{-1} could be ascribed to the alkyl-substituted ether (C–H–C) [52, 56]. The FTIR spectra of DS after CV dye adsorption (Fig. 1b) did not differ significantly from that of the material prior to adsorption, except for a few minor shifts in FTIR peak locations, which could indicate that the acidic functional groups on the surface of DS were tapped as adsorption sites for trapping the CV cationic dye molecules. The FT-IR spectra of CV-loaded DS revealed a peak at 1580 cm^{-1} assigned to the stretching vibrations of C=C distinctive to the aromatic ring of CV dye, while the peak located at 1369 cm^{-1} is ascribed to the stretching vibration of C–N distinctive to the aromatic tertiary amine [52]. As a result, the FTIR spectrum shown in Fig. 1a supports that the DS surface is richly implanted with hydroxyl and carboxylic groups which are considered active sites of CV adsorption.

The change in DS surface morphology before and after CV adsorption can be visualized by comparing their SEM images. As can be seen in Fig. 2a, the DS biomass has a rough texture and cavities of various dimensions and shapes, primarily large and wide cavities with slits. After

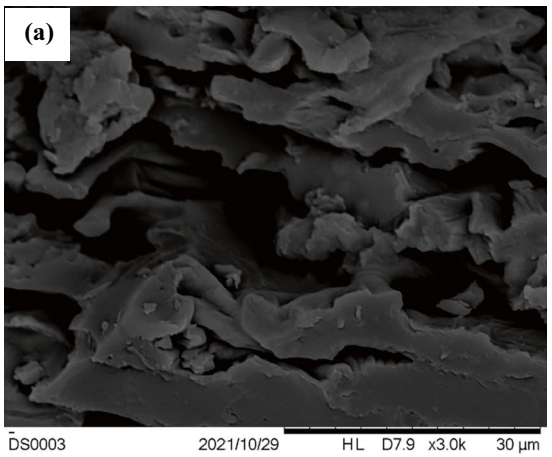

Element	AN	Series	Norm. C [wt.%]	Atom. C [at.%]
C	6	K-series	48.67	55.43
O	8	K-series	45.77	39.14
N	7	K-series	5.56	5.43
		Total:	100	100

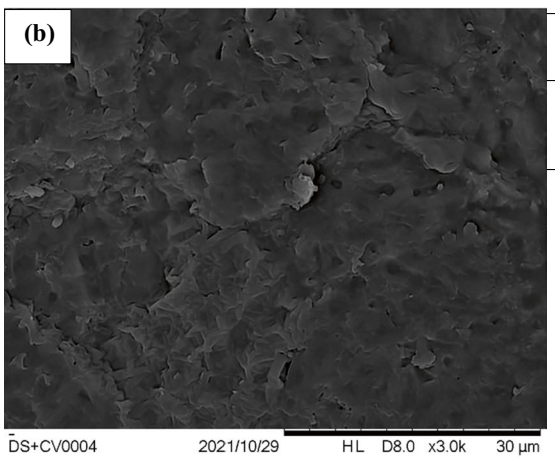

Element	AN	Series	Norm. C [wt.%]	Atom. C [at.%]
C	6	K-series	44.06	50.74
O	8	K-series	48.53	41.95
N	7	K-series	7.41	7.32
		Total:	100	100

Fig. 2 SEM images and EDX spectra of **a** DS and **b** DS after adsorption of CV dye at × 3.0k magnification

the CV adsorption, a more compact surface morphology was observed (Fig. 2b). This can be attributed to the CV molecules occupying the DS pores and cavities. The EDX examination of the DS before and after CV dye adsorption detected the presence of carbon, oxygen, and nitrogen. The changes in the element content before and after adsorption can be assigned to the CV loading onto the surface of DS.

3.2 Model fitting

Analysis of variance (ANOVA) was employed to evaluate the statistical validity of the developed nonlinear quadratic model. The ANOVA statistics for the CV removal are shown in Table 2. The ANOVA results for the suggested quadratic model showed that the employed factors are highly considerable. The high F value (59.56) and a low probability value (p-value < 0.0001) indicated the statistical significance of the model. The high coefficient of determination ($R^2 = 0.98$) value for CV dye removal (%) indicated that the model was statistically significant. As a result, the model established by BBD was appropriate for predicting the removal of CV dye within the ranges of the tested parameters. The lack of fit's insignificant p-value (0.2944) supported the validity of the used model [57]. Consequently, the operational parameters with p-values larger than 0.05 are often considered statistically irrelevant in terms of CV adsorption performance, and vice versa. Thus, the terms A, B, C, D, AB, AD, BC, and C^2 of the CV dye removal model were designated as statistically significant model terms. Furthermore, a second-order polynomial (Eq. (2)) can be used to express the relationship between the tested variables and the response:

$$CV\ removal\ (\%) = +56.18 + 27.40A + 16.02B + 6.39C + 7.47D + 4.65AB + 6.17AD + 5.72BC + 4.47C^2 \quad (2)$$

The BBD graphs aid in the validation of the established BBD model by studying the residual distribution's characteristics and identifying the degree of association between experimental and theoretical CV dye removal values. The graph of the normal probability of the residuals for the model (CV removal) is expressed in Fig. S2a. The points in Fig. S2a appear to be neatly matched with the straight line, demonstrating the points' regular and accurate distribution as well as the residuals' independence. Furthermore, Fig. S2b depicts the relationship between the theoretical and actual values of CV dye removal. From Fig. S2b, there is a strong correlation between those that are statistically predicted and the empirical output (CV removal), indicating that the model is statistically reliable [58]. Thus, Fig. S2c depicts residuals vs. run number of CV dye removal. The dots in Fig. S2c are distributed randomly around zero, showing that the model is accurate and credible.

3.3 Significant interactions

To analyze the influence of the examined inputs and identify the significant correlation between the tested parameters on the CV dye adsorption, 3D surfaces and

Table 2 Analysis of variance (ANOVA) for CV removal (%)

Source	Sum of squares	df	Mean square	F-value	p-value	Remarks
Model	14038.48	14	1002.75	59.56	< 0.0001	Significant
A-DS dose	9009.12	1	9009.12	535.14	< 0.0001	Significant
B-pH	3081.61	1	3081.61	183.05	< 0.0001	Significant
C-Temp.	490.24	1	490.24	29.12	< 0.0001	Significant
D-Time	669.01	1	669.01	39.74	< 0.0001	Significant
AB	86.49	1	86.49	5.14	0.0398	Significant
AC	21.62	1	21.62	1.28	0.2761	Not significant
AD	152.52	1	152.52	9.06	0.0094	Significant
BC	131.10	1	131.10	7.79	0.0144	Significant
BD	23.04	1	23.04	1.37	0.2616	Not significant
CD	18.92	1	18.92	1.12	0.3070	Not significant
A^2	59.95	1	59.95	3.56	0.0801	Not significant
B^2	46.50	1	46.50	2.76	0.1187	Not significant
C^2	129.75	1	129.75	7.71	0.0149	Significant
D^2	67.05	1	67.05	3.98	0.0658	Not significant
Residual	235.69	14	16.83			
Lack of fit	193.38	10	19.34	1.83	0.2944	Not significant
Pure error	42.31	4	10.58			
Cor total	14274.17	28				

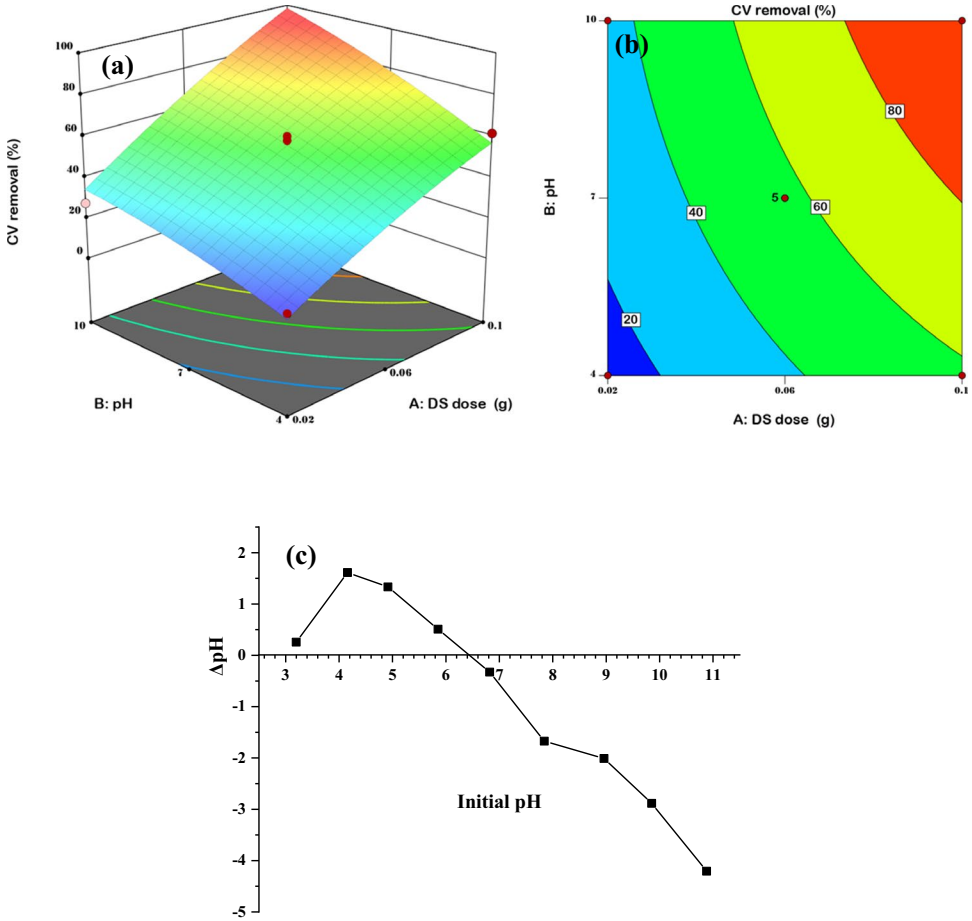

Fig. 3 Plots of **a** three-dimensional surfaces (3D) and **b** two-dimensional contour (2D) for the interaction AB (DS dose vs. pH), while **c** pH_{pzc} of DS

2D diagrams were employed. The 3D and 2D graphs of the interaction between DS dosage and pH are shown in Fig. 3a and b, respectively. The results illustrate that increasing DS dosage from 0.02 g to 0.1 g is responsible for enhancing the CV removal (%). In fact, this improvement in CV removal (%) can be assigned to the abundance of more binding sites of DS in the CV dye solution. Additionally, as shown in Fig. 3a and b, increasing the solution pH from 4 to 10 leads to an increase in the removal efficiency of CV dye. In this respect, pH_{pzc} test of DS was performed to understand the influence of pH on the adsorption of CV dye. Thus, the pH_{pzc} of DS was found to be 6.5, as shown in Fig. 3c. Consequently, at high acidic pH values, i.e., below the pH_{pzc}, the DS surface will acquire a positive charge. Therefore, at solution pH = 10, the DS surface and CV molecules become negatively and positively charged, respectively. As a result, an electrostatic attraction between the positive charge on the surface of CV dye molecules and the negative charge on the surface of DS would be possibly occurred, and the proper description of this interaction can be presented in Eq. (3):

$$DS^- + (CV) = \underset{\underset{(CH_3)}{|}}{\overset{(CH_3)}{|}}{N^+} \leftrightarrow DS^- \ldots {}^{+}\underset{\underset{(CH_3)}{|}}{\overset{(CH_3)}{|}}{N} = (CV) \quad (3)$$

Furthermore, the 3D and 2D graphs of the interaction between DS dosage and time are shown in Fig. 4a and b, respectively. The results reveal that extending the contact time from 5 to 25 min did not enhance the removal efficiency of CV dye. This observation can be ascribed to the fact that reaching the equilibrium of absorption process was achieved in a short period of time due to the functionality and effectiveness of DS surface. Moreover, the 3D and 2D graphs of the BC interaction (pH and temperature) are shown in Fig. 4c and d, respectively.

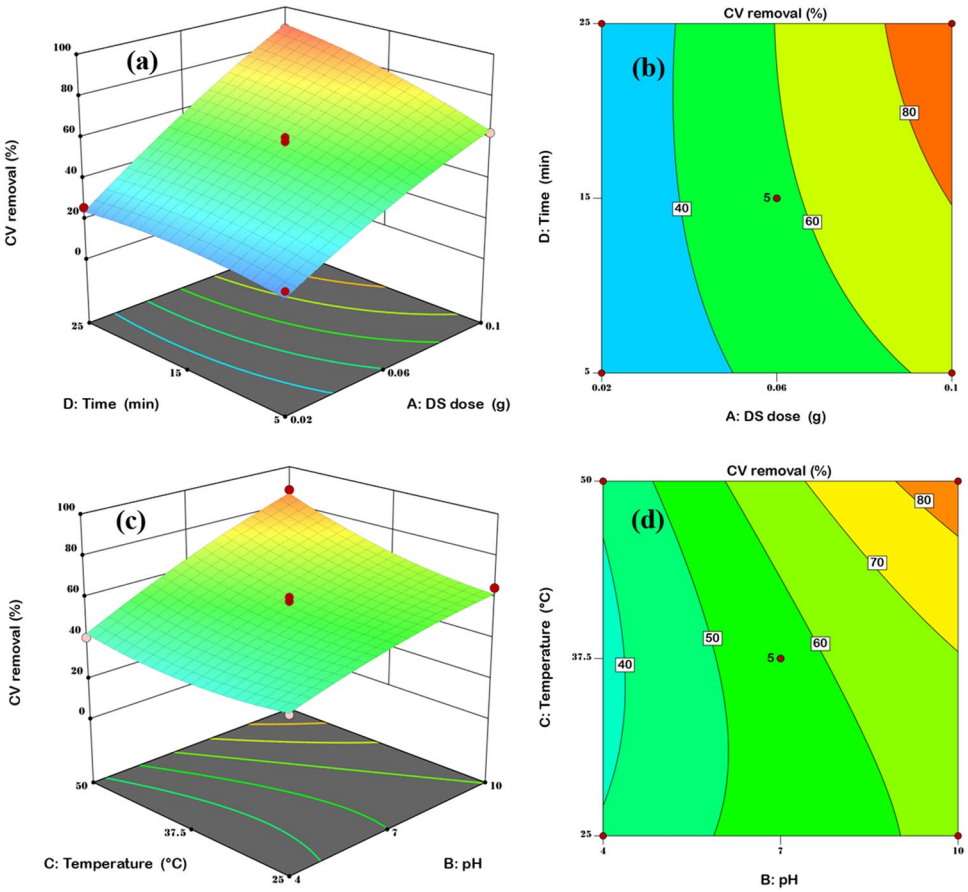

Fig. 4 **a** and **b** are 3D and 2D plots for the interaction AD (DS dose vs. time) respectively, while **c** and **d** are plots of 3D and 2D of the interaction BC (pH vs. temperature) respectively

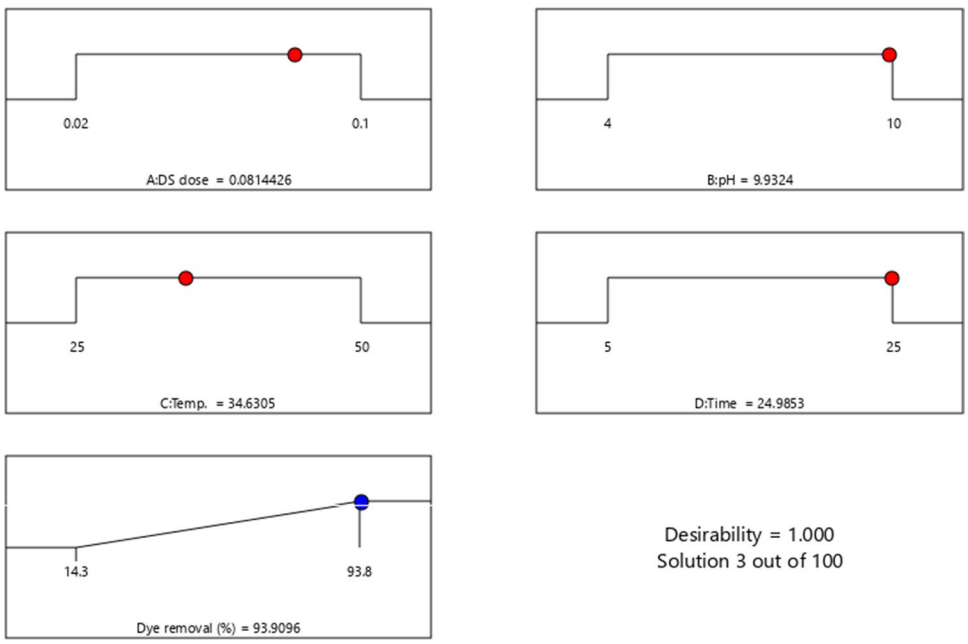

Fig. 5 Desirability ramps for the optimization of important adsorption input factors (DS dose, pH, time, and temperature) for CV dye removal (%)

The proportional relationship between the improvement of CV removal and the increases in the working temperature (25 to 50 °C) indicates that the CV adsorption process was endothermic in nature [59].

3.4 Optimization by the desirability function

The desirability function was carried out to verify the optimum operational conditions and to select the best operational conditions to achieve maximum output within the range of input variables. Thus, a desirable value of response can be attended if the desirability is equal to 1. Contrariwise, a desirability value of 0 indicates that the response value exceeds the required acceptable threshold value [60]. Subsequently, the numerical optimization shows the best operational conditions for maximum removal of CV as depicted in Fig. 5. As can be seen, the CV removal is 93.91% under the following working conditions: DS dosage of 0.081 g, pH = 9.9, temperature = 34.6 °C, and time = 24.9 min, with a desirability value of 1. Furthermore, the predictive validity of the numerical model was tested using duplicate confirmatory experiments with optimized parameters. Overall, the experimental data agreed well with the results of numerical optimization in terms of desirability functions. This result demonstrates that the desirability function can be considered a powerful tool to effectively optimize the experimental conditions of CV adsorption by DS. As a result, in subsequent studies, the optimal experimental conditions for CV adsorption were used.

3.5 Adsorption study

The adsorption study of CV by DS was carried out in batch mode. Thus, the CV uptake by DS at various interval times and with different initial CV concentrations (50, 100, 150, 200, 250, and 300 mg/L) was explored, while the three remaining parameters were left at their optimum conditions: DS dose = 0.081 g, pH = 9.9, and temperature = 34.6 °C. In this regard, the curves of the CV uptake by DS and its adsorption capacities (q_t, mg/g) at various CV concentrations are shown in Fig. 6a. As can be seen, the increment in the initial CV concentration from 50 to 300 mg/L leads to the enhancement in the adsorption capacity of DS from 59.6 to 164.0 mg/g. Hence, by increasing the initial CV concentration, the number of effective collisions between CV molecules and DS increases as well. In addition, as the initial CV concentration increased, the time to reach equilibrium increased as well.

3.6 Adsorption kinetics

The adsorption kinetic study was performed for acquiring a complete understanding of the adsorption process of CV dye

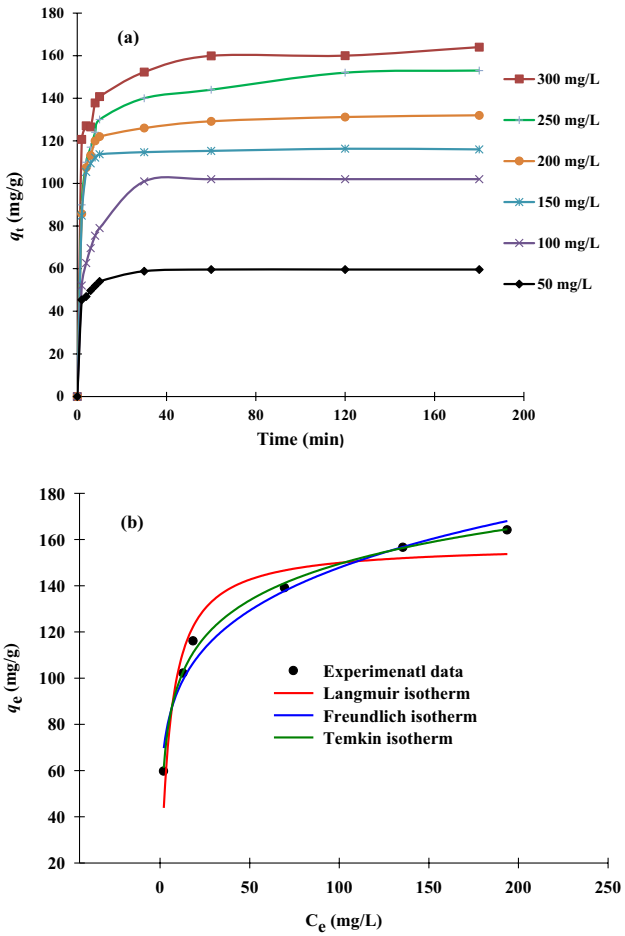

Fig. 6 **a** Effect of the contact time on CV adsorption at different initial concentrations (dose = 0.081 g, pH = 9.9, temperature = 34.6 °C, agitation speed = 100 rpm, and volume of solution = 100 mL), **b** adsorption isotherms of CV by DS (dose = 0.081 g, pH = 9.9, temperature = 34.6 °C, agitation speed = 100 rpm and volume of solution = 100 mL)

onto DS, as well as defining the rate-controlling phase that is primarily responsible for dye adsorption. The adsorption kinetics parameters were determined using two nonlinear equations namely pseudo-first order (PFO) [61] and pseudo-second order (PSO) [62]. Both formulas of PFO and PSO are given by Eqs. (4) and (5), respectively:

$$q_t = q_e\left(1 - \exp^{-k}1^t\right) \tag{4}$$

$$qt = \frac{q_e^2 k_2 t}{1 + q_e k_2 t} \tag{5}$$

where q_t indicates the amount of CV uptake (mg/g) at a time (t), and k_1 (1/min) and k_2 (g/mg min) represent the PFO, and the PSO rate constants, respectively. The estimated findings and plots for the PFO and PSO models are given in Table 3 and Fig. S3, respectively. The R^2 values

Table 3 PFO and PSO kinetic parameters for the adsorption CV on DS

Concentration (mg/L)	$q_{e\ exp.}$ (mg/g)	Pseudo-first order			Pseudo-second order		
		$q_{e\ cal.}$ (mg/g)	k_1 (1/min)	R^2	$q_{e\ cal.}$ (mg/g)	$k_2 \times 10^2$ (g/mg min)	R^2
50	59.6	54.5	0.75	0.97	58.5	2.221	0.99
100	102	96.2	0.24	0.94	103.2	0.355	0.98
150	116.3	114.1	0.66	0.98	117.8	1.272	0.99
200	139.7	127.8	0.48	0.97	136.3	0.686	0.99
250	156.0	142.5	0.37	0.95	150.8	0.436	0.99
300	164.0	149.1	0.66	0.93	159.1	0.721	0.98

Table 4 Isotherm parameters of CV adsorption by DS (dose = 0.081 g, pH = 9.9, temperature = 34.6 °C, agitation speed = 100 rpm, and volume of solution = 100 mL)

Model	Parameter	Values
Langmuir	q_{max} (mg/g)	158.0
	K_a (L/mg)	0.18
	R^2	0.93
Freundlich	K_F (mg/g (L/mg)$^{1/n}$)	16.3
	$1/n$	0.193
	R^2	0.97
Temkin	K_T (L/mg)	7.16
	b_T (J/mol)	108.9
	R^2	0.99

for PFO and PSO are close to each other, with obvious preferences towards PSO due to higher coefficient of determination value (R^2). Furthermore, the consistency between the theoretical q values (q_{cal}) of the PSO and the experimental q (q_{exp}) values reconfirmed the fitness of PSO over PFO. Overall, the chemisorption pathway drives CV adsorption on DS surface [63].

3.7 Adsorption isotherms

At constant temperature, adsorption isotherm models can be used to verify the interaction mechanisms in the adsorbent/adsorbate system. Therefore, three fundamental isotherm models, namely, Langmuir [64], Freundlich [65], and Temkin [66], were investigated. Equations (6), (7), and (8) present the non-linear formulas of the Langmuir, Freundlich, and Temkin models, respectively:

$$q_e \frac{q_{max} K_a C_e}{1 + K_a C_e} \tag{6}$$

$$q_e = K_f {C_e}^{1/n} \tag{7}$$

$$q_e = \frac{RT}{b_T} \ln (K_T C_e) \tag{8}$$

where q_{max} (mg/g) represents DS maximum adsorption capacity, q_e (mg/g) the CV uptake at equilibrium, and n the adsorption intensity. Also, K_a (L/mg), K_f (mg/g). (L/mg)$^{1/n}$, and K_T (L/mg) are Langmuir, Freundlich, and Temkin constants, respectively. Figure 6b depicts the non-linear isotherm plots of CV adsorption, and Table 4 shows all the isotherm parameters. Based on R^2 values, CV dye adsorption is well described by the Freundlich and Temkin isotherm models, indicating multilayer and heterogeneous distribution onto adsorption sites [67]. The value of $1/n$ can be used to determine the type of isotherm, such as irreversible ($1/n = 0$), favorable ($0 > 1/n < 1$), or unfavorable ($1/n > 1$). The Freundlich isotherm's $1/n$ value of 0.193 indicated a good adsorption characteristic [68]. Moreover, the obtained q_{max} from the Langmuir model was 158.0 mg/g at 34.6 °C. Considering this finding, DS can be considered as an efficient biosorbent for cationic dye removal

Table 5 A comparison of CV adsorption capacities by various adsorbents

Adsorbents	Dose	pH	q_{max} (mg/g)	References
DS	0.081 g	9.9	158	Present study
NaOH-activated *Aerva javanica* leaf	20 mg	9	315.2	[69]
Monolithic algal green powder	1.5 g	8.6	119.02	[52]
Zinc oxide nanorods loaded on activate carbon	0.025 g	7	113.64	[70]
Activated carbon from poultry litter	2.5 g	10	70.32	[71]
Zinc chloride–activated (RHZ) rice husk	5 g	10.8	61.57	[72]
Natural adsorbent black turmeric	0.03 g	9	23.753	[11]
Iron-based metal organic framework	0.03 g	6	9.259	[12]

Table 6 Thermodynamic functions for the adsorption of CV by DS (dose = 0.081 g, pH = 9.9, concentration = 100 mg/L, agitation speed = 100 rpm, and volume of solution = 100 mL)

T (K)	k_d	$\Delta G°$ (kJ/mol)	$\Delta H°$ (kJ/mol)	$\Delta S°$ (kJ/mol K)
298.15	4.06	− 3.48	18.2	0.074
308.15	7.92	− 5.30		
318.15	8.23	− 5.58		
328.15	8.35	− 5.79		

due to its high adsorption ability and simple processability compared to conventional activated adsorbents such as activated carbon. Hence, Table 5 compares the efficacy of DS in removing CV dye over other available adsorbents and indicates that DS is an alternative promising adsorbent for the removal of CV dye from aqueous environments.

3.8 Thermodynamic functions

The thermodynamic functions including standard Gibbs free energy (ΔG°), standard entropy (ΔS°), and standard enthalpy (ΔH°) were explored to provide a clear insight into the adsorption process of CV onto DS regarding spontaneity and irregularity. Hence, Eqs. (9–11) are used to compute the adsorption thermodynamic properties such as $\Delta G°$, $\Delta H°$, and $\Delta S°$ respectively [73]:

$$\Delta G° = -RTlnK_d \tag{9}$$

$$k_d = \frac{q_e}{C_e} \tag{10}$$

$$lnk_d = \frac{\Delta S°}{R} - \frac{\Delta H°}{RT} \tag{11}$$

The values of $\Delta H°$ and $\Delta S°$ were attained from the plot of ln k_d against $1/T$ (Fig. S4), which can be computed from the slope and the intercept, respectively. Thermodynamic functions for the adsorption of CV by DS are listed in Table 6. The negative values of $\Delta G°$ confirmed that the CV dye adsorption was spontaneous and increased at higher temperatures [74]. Moreover, high temperatures are desirable for the adsorption process, as shown by the fact that $\Delta G°$ for CV adsorption got higher in negative values while increasing the temperature. In fact, when $\Delta G°$ is between 400 and 80 kJ/mol, the adsorption is presumed to be chemi-adsorption. On the other hand, when $\Delta G°$ is between 20 and 0 kJ/mol, it is presumed to be physic-sorption [52]. Thus, the CV adsorption on the DS surface can be considered a physic-adsorption based on the values of $\Delta G°$ shown in Table 6. On the other hand, the positive $\Delta S°$ value indicates the DS's affinity for the CV dye, implying increased randomness. The fact that the $\Delta H°$ value is positive indicates that the CV adsorption process was endothermic in nature [75], which is consistent with the BBD findings of increased CV removal by increasing temperature.

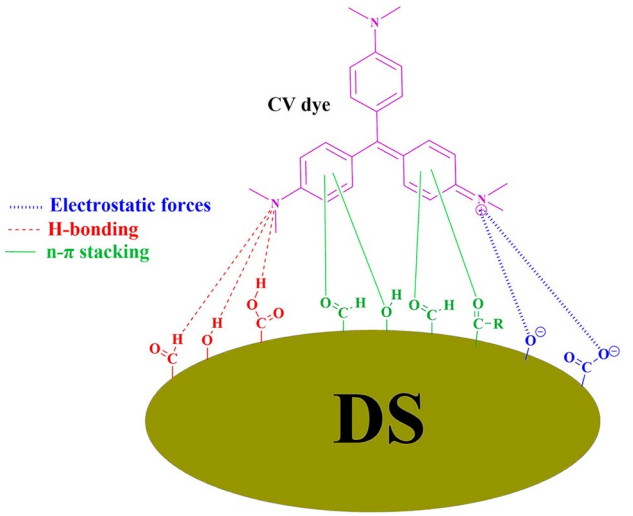

Fig. 7 Illustration of the possible interaction between DS surface and CV dye including electrostatic forces, *n*-π stacking, and H-bonding

3.9 Adsorption mechanism of CV dye

According to FTIR analysis, the surface of DS is distinguished by an abundance of active groups like hydroxyl (–OH), aldehyde (H–C=O), carboxyl (–COOH), and ketone (C=O), which agrees with previous works [51, 55]. The presence of these functional groups facilitates the predication of the adsorption mechanism of the CV dye on the surface of DS as shown in Fig. 7. The electrostatic forces were aided by the positive charge of the CV dye $\left(CV = N^{+}\left(CH_3\right)_2\right)$ and the negatively charged groups (e.g., $-COO^{-}$ and $-O^{-}$) of the DS surface. Another interaction that could occur is H-bonding between the hydrogen on the surface of DS and the nitrogen atoms present in the structure of CV dye. The *n*-π interaction is also involved in the CV adsorption through the interaction that occurs between the DS surface (oxygenated groups) and the aromatic rings of the CV dye molecules.

4 Conclusions

An alternative renewable and efficient bio-adsorbent produced from DS has been effectively employed to remove CV cationic dye from contaminated water. The optimal adsorption conditions were determined by the numerical desirability function to be DS dosage of 0.081 g, pH = 9.9, temperature = 34.6 °C, and time = 24.9 min. The kinetic results and equilibrium isotherm data illustrated that CV dye adsorption onto DS was chemisorption on the DS's multilayer heterogeneous surface. The maximal adsorption capacity of DS towards CV dye estimated from the Langmuir equation was

158 mg/g. The obtained thermodynamic values indicated that the adsorption route of CV dye by DS was spontaneous and endothermic. The adsorption mechanism of CV molecules on the surface of DS was induced by electrostatic forces, *n*-π stacking, and H-bonding interactions. This work highlights that DS can be employed as an effective and promising bio-adsorbent to remediate contaminated water with organic dyes. Furthermore, other useful applications on DS can be investigated towards removal of other categories of water contaminant such as heavy metals, pesticides, herbicides, and pharmaceutical compounds.

Supplementary Information The online version contains supplementary material available at https://doi.org/10.1007/s13399-022-03319-x.

Acknowledgements The authors would like to thank the Faculty of Applied Sciences, Universiti Teknologi MARA, Shah Alam, for all the research facilities. The author (Zeid A. ALOthman) is grateful to the Researchers Supporting Project No. (RSP-2021/1), King Saud University, Riyadh, Saudi Arabia.

Author contribution Nur Aimi Jani: formal analysis, validation, data curation. Larbi Haddad: formal analysis, validation, data curation, writing — original. Ahmed Saud Abdulhameed: formal analysis, validation, data curation, writing — original. Ali H. Jawad: conceptualization, methodology, software, supervision, project administration, writing — review and editing. Zeid A. ALOthman: validation, funding acquisition. Zaher Mundher Yaseen; formal analysis.

Data availability The datasets used and/or analyzed during the current study are available from the corresponding author on reasonable request

Declarations

Ethics approval Not applicable

Consent to participate Not applicable

Consent for publication Not applicable

Competing interests The authors declare no competing interests.

References

1. Jawad AH, Kadhum AM, Ngoh YS (2018) Applicability of dragon fruit (Hylocereus polyrhizus) peels as low-cost biosorbent for adsorption of methylene blue from aqueous solution: kinetics, equilibrium and thermodynamics studies. Desalin. Water Treat. 109:231–240. https://doi.org/10.5004/dwt.2018.21976
2. Al-Tohamy R, Ali SS, Li F, Okasha KM, Mahmoud YAG, Elsamahy T, Sun J (2022) A critical review on the treatment of dye-containing wastewater: ecotoxicological and health concerns of textile dyes and possible remediation approaches for environmental safety. Ecotoxicol Environ Safe 231:113160–113177. https://doi.org/10.1016/j.ecoenv.2021.113160
3. Javaid R, Qazi UY, Ikhlaq A, Zahid M, Alazmi A (2021) Subcritical and supercritical water oxidation for dye decomposition. J Environ Manage. 290:112605–112618. https://doi.org/10.1016/j.jenvman.2021.112605
4. Kahsay MH (2021) Synthesis and characterization of ZnO nanoparticles using aqueous extract of Becium grandiflorum for antimicrobial activity and adsorption of methylene blue. Appl Water Sci 11(2):1–12. https://doi.org/10.1007/s13201-021-01373-w
5. Allouss D, Essamlali Y, Amadine O, Chakir A, Zahouily M (2019) Response surface methodology for optimization of methylene blue adsorption onto carboxymethyl cellulose-based hydrogel beads: adsorption kinetics, isotherm, thermodynamics and reusability studies. RSC Adv 9(65):37858–37869. https://doi.org/10.1039/C9RA06450H
6. Mittal J (2020) Permissible synthetic food dyes in India. Resonance 25(4):567–577. https://doi.org/10.1007/s12045-020-0970-6
7. Rashad S, Zaki AH, Farghali AA (2019) Morphological effect of titanate nanostructures on the photocatalytic degradation of crystal violet. Nanomater Nanotechnol 9:1–10. https://doi.org/10.1177/1847980418821778
8. Mittal A, Mittal J, Malviya A, Kaur D, Gupta VK (2010) Adsorption of hazardous dye crystal violet from wastewater by waste materials. J colloid Inter Sci 343(2):463–473. https://doi.org/10.1016/j.jcis.2009.11.060
9. Mittal J, Ahmad R, Ejaz MO, Mariyam A, Mittal A (2022) A novel, eco-friendly bio-nanocomposite (Alg-Cst/Kal) for the adsorptive removal of crystal violet dye from its aqueous solutions. Int J Phyt 24(8):796–807. https://doi.org/10.1080/15226514.2021.1977778
10. He Q, Tan C, Zhang H (2017) Recent advances in cantilever-free scanning probe lithography: high-throughput, space-confined synthesis of nanostructures and beyond. ACS Nano 11(5):4381–4386. https://doi.org/10.1021/acsnano.7b03143
11. Patel A, Soni S, Mittal J, Mittal A, Arora C (2021) Sequestration of crystal violet from aqueous solution using ash of black turmeric rhizome. Desalin Water Treat 220:342–52. https://doi.org/10.5004/dwt.2021.26911
12. Soni S, Bajpai PK, Bharti D, Mittal J, Arora C (2020) Removal of crystal violet from aqueous solution using iron based metal organic framework. Desalin Water Treat 205:386–399. https://doi.org/10.5004/dwt.2020.26387
13. Cinperi NC, Ozturk E, Yigit NO, Kitis M (2019) Treatment of woolen textile wastewater using membrane bioreactor, nanofiltration and reverse osmosis for reuse in production processes. J Clean Prod 223:837–848. https://doi.org/10.1016/j.jclepro.2019.03.166
14. Li Y, An Y, Zhao R, Zhong Y, Long S, Yang J, Zheng H (2022) Synergetic removal of oppositely charged dyes by co-precipitation and amphoteric self-floating capturer: mechanism investigation by molecular simulation. Chemosphere 296:134033–134042. https://doi.org/10.1016/j.chemosphere.2022.134033
15. Rajala K, Grönfors O, Hesampour M, Mikola A (2020) Removal of microplastics from secondary wastewater treatment plant effluent by coagulation/flocculation with iron, aluminum and polyamine-based chemicals. Water Res 183:116045–116054. https://doi.org/10.1016/j.watres.2020.116045
16. Sinha AK, Sasmal AK, Pal A, Pal D, Pal T (2021) Ammonium phosphomolybdate $[(NH_4)_3PMo_{12}O_{40}]$ an inorganic ion exchanger for environmental application for purification of dye contaminant wastewater. J Photochem Photobiol A: Chem 418:113427–113436. https://doi.org/10.1016/j.jphotochem.2021.113427
17. Nozad E, Marjani AP, Mahmoudian M (2022) A novel and facile semi-IPN system in fabrication of solvent resistant nano-filtration membranes for effective separation of dye contamination in water and organic solvents. Sep Puri Technol 282:120121–120135. https://doi.org/10.1016/j.seppur.2021.120121
18. Machado GR, Carleer R, Arada PM, Gryglewicz G, Maggen J, Haeldermans T, Yperman J (2020) Adsorption of

Cibacron Yellow F-4G dye onto activated carbons obtained from peanut hull and rice husk: kinetics and equilibrium studies. Biomass Conver Bio 12:323–339. https://doi.org/10.1007/s13399-020-00699-w
19. Guo X, Jia J, Gao P, Zhang T, Zha F, Tang X, Zuo Z (2022) Flower-like $FeMoO_4$@1T-MoS_2 micro-sphere for effectively cleaning binary dyes via photo-Fenton oxidation. J Colloid Inter Sci 622:284–297. https://doi.org/10.1016/j.jcis.2022.04.113
20. Tee GT, Gok XY, Yong WF (2022) Adsorption of pollutants in wastewater via biosorbents, nanoparticles and magnetic biosorbents: a review. Environ Res. 212:113248–113268. https://doi.org/10.1016/j.envres.2022.113248
21. Munagapati VS, Wen HY, Vijaya Y, Wen JC, Wen JH, Tian Z, Raul Garcia J (2021) Removal of anionic (Acid Yellow 17 and amaranth) dyes using aminated avocado (Persea americana) seed powder: adsorption/desorption, kinetics, isotherms, thermodynamics, and recycling studies. Int J Phytoremediation 23(9):911–923. https://doi.org/10.1080/15226514.2020.1866491
22. Jawad AH, Abdulhameed AS, Bahrudin NN, Hum NNMF, Surip SN, Syed-Hassan SSA, Sabar S (2021) Microporous activated carbon developed from KOH activated biomass waste: surface mechanistic study of methylene blue dye adsorption. Water Sci Technol 84(8):1858–1872. https://doi.org/10.2166/wst.2021.355
23. Gupta VK, Agarwal S, Ahmad R, Mirza A, Mittal J (2020) Sequestration of toxic congo red dye from aqueous solution using ecofriendly guar gum/activated carbon nanocomposite. Int J Boil Macromol. 158:1310–1318. https://doi.org/10.1016/j.ijbiomac.2020.05.025
24. Mittal J (2021) Recent progress in the synthesis of layered double hydroxides and their application for the adsorptive removal of dyes: a review. J Environ Manage 295:113017–113057. https://doi.org/10.1016/j.jenvman.2021.113017
25. Mittal A, Mittal J (2015) Hen feather: a remarkable adsorbent for dye removal. Green chemistry for dyes removal from wastewater. Green Chemistry for Dyes Removal from Wastewater: Research Trends and Applications 409-457.https://doi.org/10.1002/9781118721001
26. Mittal J, Mariyam A, Sakina F, Baker RT, Sharma AK, Mittal A (2021) Batch and bulk adsorptive removal of anionic dye using metal/halide-free ordered mesoporous carbon as adsorbent. J Clean Prod 321:129060–129074. https://doi.org/10.1016/j.jclepro.2021.129060
27. Mariyam A, Mittal J, Sakina F, Baker RT, Sharma AK, Mittal A (2021) Efficient batch and fixed-bed sequestration of a basic dye using a novel variant of ordered mesoporous carbon as adsorbent. Arab J Chem 14(6):103186–103201. https://doi.org/10.1016/j.arabjc.2021.103186
28. Jawad AH, Abdulhameed AS, Hanafiah MAKM, ALOthman ZA, Khan MR, Surip SN, (2021) Numerical desirability function for adsorption of methylene blue dye by sulfonated pomegranate peel biochar: modeling, kinetic, isotherm, thermodynamic, and mechanism study. Korean J Chem Eng 38(7):1499–1509. https://doi.org/10.1007/s11814-021-0801-9
29. Abdulhameed AS, Jawad AH, Ridwan M, Khadiran T, Wilson LD, Yaseen ZM (2022) Chitosan/carbon-doped TiO_2 composite for adsorption of two anionic dyes in solution and gaseous SO_2 capture: experimental modeling and optimization. J Polym Environ 1-18. https://doi.org/10.1007/s10924-022-02532-z
30. Kumar V, Saharan P, Sharma AK, Umar A, Kaushal I, Mittal A, Rashad B (2020) Silver doped manganese oxide-carbon nanotube nanocomposite for enhanced dye-sequestration: isotherm studies and RSM modelling approach. Ceram Int 46(8):10309–10319. https://doi.org/10.1016/j.ceramint.2020.01.025
31. Pitchay T, Jawad AH, Johari IS, Sabar S (2022) Kinetics studies of metallic ions adsorption by immobilised chitosan. Sci Lett 16(1):137–148. https://doi.org/10.24191/sl.v16i1.15932
32. Mubarak A, Shazwani N, Sabar S, Jawad AH (2020) The study of commercial titanium dioxide (TiO_2) degussa P25 for the adsorption of acidic dye. Sci Lett. 14(1):68–83. https://doi.org/10.24191/sl.v14i1.10607
33. Rivera-Utrilla J, Sánchez-Polo M, Gómez-Serrano V, Álvarez PM, Alvim-Ferraz MCM, Dias JM (2011) Activated carbon modifications to enhance its water treatment applications. An overview. J Hazard Mater 187:1–23. https://doi.org/10.1016/j.jhazmat.2011.01.033
34. Reddy MS, Nirmala V, Ashwini C (2017) Bengal Gram Seed Husk as an adsorbent for the removal of dye from aqueous solutions–batch studies. Arab J Chem 10:S2554–S2566. https://doi.org/10.1016/j.arabjc.2013.09.029
35. Sidiqua MA, Priya VS (2021) Removal of yellow dye using composite binded adsorbent developed using natural clay and activated carbon from sapindus seed. Bio Agri Biotechnol 33:101965-1–1973. https://doi.org/10.1016/j.bcab.2021.101965
36. Bukhari A, Ijaz I, Zain H, Gilani E, Nazir A, Bukhari A, Iram S (2022) Removal of eosin dye from simulated media onto lemon peel-based low cost biosorbent. Arab J Chem. 15(7):103873–103885. https://doi.org/10.1016/j.arabjc.2022.103873
37. Fazal T, Faisal A, Mushtaq A, Hafeez A, Javed F, Alaud DA, Rehman F (2021) Macroalgae and coal-based biochar as a sustainable bioresource reuse for treatment of textile wastewater. Biomass Conver Bio 11(5):1491–1506. https://doi.org/10.1007/s13399-019-00555-6
38. Gayathiri M, Pulingam T, Lee KT, Sudesh K (2022) Activated carbon from biomass waste precursors: factors affecting production and adsorption mechanism. Chemosphere 294:133764–133776. https://doi.org/10.1016/j.chemosphere.2022.133764
39. Elgarahy AM, Elwakeel KZ, Mohammad SH, Elshoubaky GA (2021) A critical review of biosorption of dyes, heavy metals and metalloids from wastewater as an efficient and green process. Clean Eng Technol 4:100209–100214. https://doi.org/10.1016/j.clet.2021.100209
40. Shalaby SM, Madkour FF, El-Kassas HY, Mohamed A, Elgarahy AM (2021) Green synthesis of recyclable iron oxide nanoparticles using Spirulina platensis microalgae for adsorptive removal of cationic and anionic dyes. Environ Sci and Pollut Res 28(46):65549–65572. https://doi.org/10.1007/s11356-021-15544-4
41. Liu F, Sai KCKV, Zhang W (2021) Conversion of spiky sweetgum tree (Liquidambar styraciflua) seeds as into bioadsorbent: static and dynamic adsorption assessment. J Hazard Mater Adva 1:100001–100011. https://doi.org/10.1016/j.hazadv.2021.100001
42. Bhatta LKG, Venkatesh K, Kiran N, Gundanna SK, Bhatta UM (2021) Synthesis and characterization of activated carbon from Delonix regia seeds for CO_2 adsorption. Energy Climate Change 2:100064–100072. https://doi.org/10.1016/j.egycc.2021.100064
43. Soliman KN, Moustafa AF, Aboud AA, Halim KSA (2019) Effective utilization of Moringa seeds waste as a new green environmental adsorbent for removal of industrial toxic dyes. J Mater Res Technol 8(2):1798–1808. https://doi.org/10.1016/j.jmrt.2018.12.010
44. Wang Q, Wang Y, Yang Z, Han W, Yuan L, Zhang L, Huang X (2022) Efficient removal of Pb (II) and Cd (II) from aqueous solutions by mango seed biosorbent. Chem Eng J Adv 11:100295–100305. https://doi.org/10.1016/j.ceja.2022.100295
45. Ezekoye OM, Akpomie KG, Eze SI, Chukwujindu CN, Ani JU, Ujam OT (2020) Biosorptive interaction of alkaline modified Dialium guineense seed powders with ciprofloxacin in contaminated solution: central composite, kinetics, isotherm, thermodynamics, and desorption. Int J Phytoremediation 22(10):1028–1037. https://doi.org/10.1080/15226514.2020.1725869
46. Berry SK (1980) Cyclopropene fatty acids in some Malaysian edible seeds and nuts: I Durian (Durio zibethinus Murr). Lipids 15(6):452–455. https://doi.org/10.1007/BF02534071
47. Manshor MR, Anuar H, Aimi MN, Fitrie MA, Nazri WW, Sapuan SM, Wahit MU (2014) Mechanical, thermal and

morphological properties of durian skin fibre reinforced PLA biocomposites. Mater Design 59:279–286. https://doi.org/10.1016/j.matdes.2014.02.062
48. Lee MC, Koay SC, Chan MY, Pang MM, Chou PM, Tsai KY (2018) Preparation and characterization of durian husk fiber filled polylactic acid biocomposites. MATEC Web Conf 152:02007–02014. https://doi.org/10.1051/matecconf/201815202007
49. Dalvand A, Nabizadeh R, Ganjali MR, Khoobi M, Nazmara S, Mahvi AH (2016) Modeling of Reactive Blue 19 azo dye removal from colored textile wastewater using L-arginine-functionalized Fe_3O_4 nanoparticles: optimization, reusability, kinetic and equilibrium studies. J Magnet Magnet Mater 404:179–189. https://doi.org/10.1016/j.jmmm.2015.12.040
50. Sing KS (1985) Reporting physisorption data for gas/solid systems with special reference to the determination of surface area and porosity (Recommendations 1984). Pure Appl Chem 57(4):603–619. https://doi.org/10.1351/pac198557040603
51. Kanjana K, Harding P, Kwamman T, Kingkam W, Chutimasakul T (2021) Biomass-derived activated carbons with extremely narrow pore size distribution via eco-friendly synthesis for supercapacitor application. Biomass Bioenergy 153:106206–106218. https://doi.org/10.1016/j.biombioe.2021.106206
52. Elgarahy AM, Elwakeel KZ, Elshoubaky GA, Mohammad SH (2019) Microwave-accelerated sorption of cationic dyes onto green marine algal biomass. Environ Sci Pollution Res 26(22):22704–22722. https://doi.org/10.1007/s11356-019-05417-2
53. Ahmad MA, Ahmad N, Bello OS (2015) Modified durian seed as adsorbent for the removal of methyl red dye from aqueous solutions. Appl Water Sci 5(4):407–423. https://doi.org/10.1007/s13201-014-0208-4
54. González-García P, Centeno TA, Urones-Garrote E, Ávila-Brande D, Otero-Díaz LC (2013) Microstructure and surface properties of lignocellulosic-based activated carbons. Appl Surf Science 265:731–737. https://doi.org/10.1016/j.apsusc.2012.11.092
55. Ahmad MA, Ahmad N, Bello OS (2014) Adsorptive removal of malachite green dye using durian seed-based activated carbon. Water Air Soil Pollut 225(8):1–18. https://doi.org/10.1007/s11270-014-2057-z
56. Elwakeel KZ, Elgarahy AM, Elshoubaky GA, Mohammad SH (2020) Microwave assist sorption of crystal violet and Congo red dyes onto amphoteric sorbent based on upcycled Sepia shells. J Environ Health Sci Eng 18(1):35–50. https://doi.org/10.1007/s40201-019-00435-1
57. Kutluay S, Temel F (2021) Silica gel based new adsorbent having enhanced VOC dynamic adsorption/desorption performance. Colloids Surf A: Physicochem Eng Asp 609:125848–125862. https://doi.org/10.1016/j.colsurfa.2020.125848
58. Jawad AH, Abdulhameed AS, Wilson LD, Hanafiah MAKM, Nawawi WI, ALOthman ZA, Rizwan Khan M, (2021) Fabrication of schiff's base chitosan-glutaraldehyde/activated charcoal composite for cationic dye removal: optimization using response surface methodology. J Polym Environ 29(9):2855–2868. https://doi.org/10.1007/s10924-021-02057-x
59. Shooto ND (2020) Removal of toxic hexavalent chromium (Cr (VI)) and divalent lead (Pb (II)) ions from aqueous solution by modified rhizomes of Acorus calamus. Surf Interface 20:100624–100633. https://doi.org/10.1016/j.surfin.2020.100624
60. Mourabet M, El Rhilassi A, El Boujaady H, Bennani-Ziatni M, El Hamri R, Taitai A (2012) Removal of fluoride from aqueous solution by adsorption on Apatitic tricalcium phosphate using Box-Behnken design and desirability function. Appl Surf Sci 258(10):4402–4410. https://doi.org/10.1016/j.apsusc.2011.12.125
61. Lagergren S (1898) Zur theorie der sogenannten adsorption geloster stoffe. Vet. Akad. Handl. 24:1–39
62. Ho YS, McKay G (1998) Sorption of dye from aqueous solution by peat. Chem Eng J 70:115–124. https://doi.org/10.1016/S0923-0467(98)00076-1
63. Qin P, Chen D, Li M, Li D, Gao Y, Zhu S, Lu M (2022) Melamine/MIL-101 (Fe)-derived magnetic carbon nanotube-decorated nitrogen-doped carbon materials as sorbent for rapid removal of organic dyes from environmental water sample. J Mol Liq 359:119231–119241. https://doi.org/10.1016/j.molliq.2022.119231
64. Langmuir I (1918) The adsorption of gases on plane surfaces of glass, mica and platinum. J Am Chem Soc 40:1361–1403. https://doi.org/10.1021/ja02242a004
65. Freundlich HMF (1906) Over the adsorption in solution. J Phys Chem 57:385–471
66. Temkin MI (1940) Kinetics of ammonia synthesis on promoted iron catalysts. Acta physiochim URSS 12:327–356
67. Siddiqui MN, Chanbasha B, Al-Arfaj AA, Kon'kova T, Ali I, (2021) Super-fast removal of cobalt metal ions in water using inexpensive mesoporous carbon obtained from industrial waste material. Environ Technol Innov 21:101257–101271. https://doi.org/10.1016/j.eti.2020.101257
68. Hoseinzadeh H, Hayati B, Ghaheh FS, Seifpanahi-Shabani K, Mahmoodi NM (2021) Development of room temperature synthesized and functionalized metal-organic framework/graphene oxide composite and pollutant adsorption ability. Mater Res Bullet 142:111408–111419. https://doi.org/10.1016/j.materresbull.2021.111408
69. AL-Shehri, HS, Almudaifer E, Alorabi AQ, Alanazi, HS, Alkorbi AS, Alharthi FA (2021) Effective adsorption of crystal violet from aqueous solutions with effective adsorbent: equilibrium, mechanism studies and modeling analysis. Environmental Pollut Bio 33(1):214-226.https://doi.org/10.1080/26395940.2021.1960199
70. Dil EA, Ghaedi M, Ghaedi A, Asfaram A, Jamshidi M, Purkait MK (2016) Application of artificial neural network and response surface methodology for the removal of crystal violet by zinc oxide nanorods loaded on activate carbon: kinetics and equilibrium study. J Taiwan Inst Chem Eng 59:210–220. https://doi.org/10.1016/j.jtice.2015.07.023
71. Yusuff AS, Ajayi OA, Popoola LT (2021) Application of Taguchi design approach to parametric optimization of adsorption of crystal violet dye by activated carbon from poultry litter. Sci African 13:e00850–e00863. https://doi.org/10.1016/j.sciaf.2021.e00850
72. Mohanty K, Naidu JT, Meikap BC, Biswas MN (2006) Removal of crystal violet from wastewater by activated carbons prepared from rice husk. Ind Eng Chem Res 45(14):5165–5171. https://doi.org/10.1021/ie060257r
73. Jawad AH, Abdulhameed AS, Surip SN, Sabar S (2020) Adsorptive performance of carbon modified chitosan biopolymer for cationic dye removal: kinetic, isotherm, thermodynamic, and mechanism study. Int J Environ Anal Chem 28:1–15. https://doi.org/10.1080/03067319.2020.1807966
74. Sinha R, Kumar R, Abhishek K, Shang J, Bhattacharya S, Sengupta S, Sharma P (2022) Single-step synthesis of activated magnetic biochar derived from rice husk for hexavalent chromium adsorption: equilibrium mechanism, kinetics, and thermodynamics analysis. Groundwater Sustain Develop 18:100796–100809. https://doi.org/10.1016/j.gsd.2022.100796
75. Kumari B, Tiwary RK, Yadav M, Singh KMP (2021) Nonlinear regression analysis and response surface modeling of Cr (VI) removal from synthetic wastewater by an agro-waste Cocos Nucifera: Box-Behnken Design (BBD). Int J Phytoremediation 23(8):791–808. https://doi.org/10.1080/15226514.2020.1858399